The Journal of Chemical Physics

The quantum structure of anionic hydrogen clusters

Cite as: J. Chem. Phys. **148**, 102305 (2018); https://doi.org/10.1063/1.4990612
Submitted: 16 June 2017 . Accepted: 27 July 2017 . Published Online: 06 September 2017

F. Calvo, and E. Yurtsever

View Online Export Citation CrossMark

ARTICLES YOU MAY BE INTERESTED IN

Isotope effects in aqueous solvation of simple halides
The Journal of Chemical Physics **148**, 102306 (2018); https://doi.org/10.1063/1.4986231

A comparative study of different methods for calculating electronic transition rates
The Journal of Chemical Physics **148**, 102304 (2018); https://doi.org/10.1063/1.4989509

Quantum mechanical free energy profiles with post-quantization restraints: Binding free energy of the water dimer over a broad range of temperatures
The Journal of Chemical Physics **148**, 102303 (2018); https://doi.org/10.1063/1.4986915



AIP Publishing

© 2018 Author(s).

The quantum structure of anionic hydrogen clusters

F. Calvo[1,a] and E. Yurtsever[2]
[1]*University Grenoble Alpes, LIPHY, F-38000 Grenoble, France and CNRS, LIPHY, F-38000 Grenoble, France*
[2]*Koç University, Rumelifeneriyolu, Sariyer, Istanbul 34450, Turkey*

(Received 16 June 2017; accepted 27 July 2017; published online 6 September 2017)

A flexible and polarizable interatomic potential has been developed to model hydrogen clusters interacting with one hydrogen anion, $(H_2)_nH^-$, in a broad range of sizes n = 1–54 and parametrized against coupled cluster quantum chemical calculations. Using path-integral molecular dynamics simulations at 1 K initiated from the putative classical global minima, the equilibrium structures are found to generally rely on icosahedral shells with the hydrogen molecules pointing toward the anion, producing geometric magic numbers at sizes n = 12, 32, and 44 that are in agreement with recent mass spectrometry measurements. The energetic stability of the clusters is also connected with the extent of vibrational delocalization, measured here by the fluctuations among inherent structures hidden in the vibrational wave function. As the clusters grow, the outer molecules become increasingly free to rotate, and strong finite size effects are also found between magic numbers, associated with more prominent vibrational delocalization. The effective icosahedral structure of the 44-molecule cluster is found to originate from quantum nuclear effects as well, the classical structure showing no particular symmetry. *Published by AIP Publishing.* [http://dx.doi.org/10.1063/1.4990612]

I. INTRODUCTION

Hydrogen clusters can be produced in neutral or cationic (protonated) form but, until fairly recently, not in anionic form except for H^- itself. H_2^- is unstable, and although theoretically predicted as stable for a long time,[1–3] H_3^- was conclusively identified only during the last decade in experiments on dielectric discharge plasmas by Wang and co-workers.[4] Larger anionic clusters turn out to be very elusive and were first produced inside the cryogenic medium of helium droplets by Renzler and co-workers.[5]

The general interest behind hydrogen clusters stems from their relative chemical simplicity, their constituents being only electrons and protons. This makes them natural model systems to investigate the relation between structure, bonding, and spectroscopy, especially in the case of protonated clusters where electronic delocalization combines with quantum nuclear effects to produce a rich dynamics.[6,7,15,16] Neutral hydrogen clusters have been scrutinized mostly in relation with the suggestion that superfluidity could arise in such low density materials, crystallinity preventing bulk hydrogen from reaching the superfluid state upon cooling.[8] Although still unconfirmed experimentally, computational studies have provided strong evidence that indeed the bosonic nature of *para*-hydrogen should set in at sufficiently low temperatures yet without destroying completely the overall molecular structure.[9] Such so-called supersolid states have also been reported in *para*-hydrogen clusters deposited on surfaces.[10]

Because they are made from the most abundant element in the universe, hydrogen clusters have unsurprisingly been observed in astrophysical environments with the notable examples of the protonated compounds, H_3^+ playing a pivotal role in astrochemistry ranging from planetary atmospheres[11,12] to molecular[13] or diffuse[14] interstellar clouds. Anionic clusters, which are expected to be more bound than neutrals owing to polarization forces, could also well be present as the result of electron collisions on hydrogen clusters, followed by nucleation and growth on the anionic seed.

A major step toward understanding the physics and chemistry of anionic hydrogen clusters was achieved by a mass spectrometry experiment in which H_N^- clusters and their fully deuterated forms were detected up to sizes exceeding $N > 120$ atoms.[5] Only odd-sized clusters were observed, consistently with the very short-lived nature of H_2^- (Ref. 17) and its existence mainly as a metastable intermediate. Among even-sized compounds, mass spectrometry reveals drops in abundances above sizes N of 25, 65, and, albeit to a slightly lesser extent, 89.[5] Quantum chemistry calculations[18–21] have confirmed that small clusters adopt a clear molecular structure in which H_2 molecules point toward H^-, with a reasonably strong binding originating from electrostatic and polarization forces. This scheme explains the magic size at $N = 25$ as an icosahedral shell of H_2 molecules surrounding the anion, as also confirmed by density functional theory (DFT) calculations.[21] The other two magic numbers of 65 and 89 were interpreted as the result of geometric shell filling respecting icosahedral symmetry, with 20 additional molecules forming a dodecahedral cage around the initial shell, and a third icosahedral shell above it. In other cryogenic media such as helium droplets, the stronger interaction experienced by the charged impurity and the solvent is responsible for the formation of the so-called snowballs in which the immediately surrounding layer freezes and localizes, superfluidity being also suppressed. Such effects have

[a]Electronic mail: florent.calvo@univ-grenoble-alpes.fr

been evidenced experimentally by mass spectrometry[22] but also computationally and for both cationic[23–26] and anionic[27] dopants.

Although the potential energy surfaces explored by methods explicitly accounting for electronic structure are likely to be accurate, hydrogen clusters as studied in Ref. 5 are extremely light and cold, hence strongly prone to vibrational delocalization and other nuclear quantum effects. The goal of the present paper is to theoretically investigate the structure of such anionic hydrogen clusters, including a rigorous description of nuclear quantum effects beyond the harmonic approximation through path-integral molecular dynamics (PIMD) simulations. In order to deal with clusters containing up to about 100 atoms, a polarizable and flexible force field was constructed based on well-established components and parametrized on dedicated quantum chemical calculations. Before its implementation within the PIMD framework, putative global minima of the potential energy surfaces were located, and a variety of quantities were determined to characterize the structural features of $(H_2)_nH^-$ clusters for $n = 1$–54 and their deuterated analogues. Our results confirm the multilayer icosahedral nature and show that at 1 K, the rotational motion of individual hydrogen molecules is suppressed due to a strong alignment toward the central H^- ion. Nuclear quantum effects appear essential in stabilizing the icosahedral arrangement in larger clusters, classical structures being too compact and with lower symmetry.

The article is organized as follows. In Sec. II, we describe the various elements of the potential energy surface, the method to locate the putative global minima, and the details of the PIMD simulations, including the main observables considered to characterize the quantum structure. In Sec. III, we present and discuss our main results, emphasizing remarkably stable systems and occasionally illustrating cluster size effects.[28] We finally give some concluding remarks in Sec. IV.

II. METHODS

At very low temperatures, neutral (*para*-)hydrogen clusters or clusters weakly bound to a molecular impurity can generally be described as coarse-grained point particles owing to the minor extension of H_2 relative to intermolecular distances and those lying in the $J = 0$ rovibrational ground state in which the rotational wave function is isotropic. We first attempted to model $(H_2)_nH^-$ clusters in a similar way, using the commonly employed Silvera-Goldman effective pair potential[29] between H_2 molecules and a similar form for the H_2–H^- interaction added to a polarization term. Unfortunately, such a simplified potential gave qualitatively wrong cluster structures (*vide infra*) and a more realistic all-atom model suitable for PIMD simulations was developed instead.

A. Potential energy surface

The polarizable potential developed in this work for H_N^- clusters relies on existing components for the interaction between H_2 molecules, to which we only added some flexibility, and a minimum number of parameters for the H_2–H^- interaction. The potential was constructed with structural properties in mind, rather than accurate energetics or spectroscopy, and much more realistic potentials[30] are available, e.g., H_2–H_2, but they would not be practical for large hydrogen clusters.

H_N^- clusters with $N = 2n + 1$ clusters are modeled assuming no charge transfer between the anion and the hydrogen molecules, but polarization interactions through a single polarization site carried by the molecules at their center. H_2 molecules themselves are described as flexible through an intramolecular potential $V_{\rm intra}(r)$ that depends on the internuclear distance r via a Rydberg expression,

$$V_{\rm intra}(r) = V_0\left[1 - \left(1 + \rho + \delta_{H_2}\rho^3\right)\exp(-\rho)\right],$$
$$\rho(r) = a_{H_2}\left(\frac{r}{r_{H_2}} - 1\right). \quad (1)$$

This potential was least-squared fitted on dedicated quantum chemistry calculations performed at the coupled cluster level with single, double, and perturbative triple [CCSD(T)] excitations, extrapolated at the complete basis set (CBS) limit from data obtained for the basis sets aug-cc-pVTZ, aug-cc-pVQZ, and aug-cc-pV5Z, and further corrected for basis set superposition errors. Figure 1 shows the results obtained with such an explicit treatment of the electronic structure and the fitted potential.

Interactions between hydrogen molecules were modeled following the work of Darkrim and Levesque[31,32] who developed a potential designed for bulk H_2, which comprises isotropic repulsion-dispersion terms and a quadrupolar component that turns out to be essential also for modeling the interaction with the hydrogen anion. To model quadrupolar interactions, the two hydrogen sites carry a partial charge $+q$ each, the molecular center carrying $-2q$. The value of $q = 0.4829e$ was taken from Ref. 31. In addition to direct electrostatic interactions between the H^- anion and the various hydrogen molecules, an isotropic repulsion-dispersion term $V_{\rm inter}^{H_2-H_2}(r)$ is acting between any pair of H_2 molecules at their centers, using here a simple but appropriate Lennard-Jones (LJ) form also taken from the work

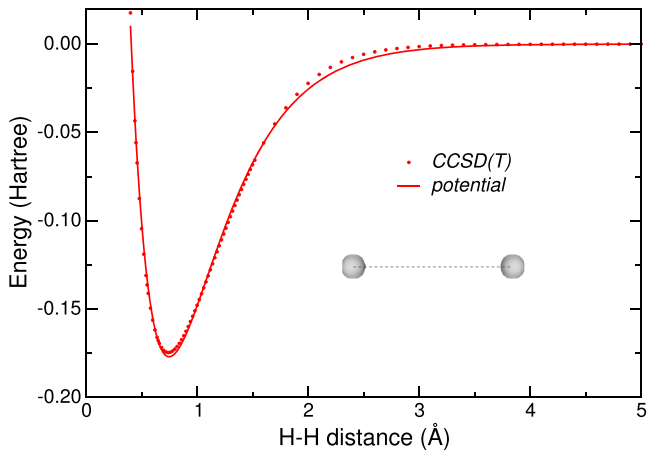


FIG. 1. Potential energy curve of the hydrogen dimer in its ground electronic state, as obtained from CCSD(T) calculations at the complete basis set limit (circles) or from the present Rydberg potential (solid lines).

of Darkrim and Levesque.[31] The non-electrostatic interaction $V_{\text{inter}}^{\text{H}_2\text{–H}^-}(r)$ between H^- and each H_2 molecule is described using a more flexible Buckingham-type potential acting again at the molecular center of H_2,

$$V_{\text{inter}}^{\text{H}_2\text{–H}^-}(r) = A\exp(-br) - f_{\text{cut}}(r)\left[\frac{C_6}{r^6} + \frac{C_8}{r^8}\right], \quad (2)$$

where $f_{\text{cut}}(r)$ is a damping function needed to prevent short-range divergence of the potential below the distance r_{cut},

$$f_{\text{cut}}(r) = \begin{cases} 1, & r > r_{\text{cut}}, \\ \exp\left[-\left(1 - \frac{r_{\text{cut}}}{r}\right)\right], & r \le r_{\text{cut}}. \end{cases} \quad (3)$$

Finally, each hydrogen molecule was given a polarizable site at its center, the polarization energy of molecule i being approximated at its lowest vectorial order (i.e., without interactions between induced dipoles) as

$$V_{\text{pol}}^{(i)} = -\frac{1}{2}\alpha_{\text{H}_2}\vec{E}_i^2, \quad (4)$$

$$\vec{E}_i = \sum_{j\neq i, j\in \text{H}_2,\text{H}^-} \phi_{\text{cut}}(r)\frac{q_j\vec{r}_{ij}}{r_{ij}^3}, \quad (5)$$

where $\alpha_{\text{H}_2} = 0.787$ Å^3 is the isotropic polarizability of H_2,[33] $\vec{E}_i$ is the electric field, and q_j is the charge carried at site j by other hydrogen molecules or the H^- anion. A second damping function $\phi_{\text{cut}}(r)$ was introduced here to avoid polarization catastrophe at short range, with a similar expression as in Eq. (3) but a different cutoff parameter r_{damp}.

The anion itself also carries a polarizable site in response to the surrounding partial charges on the hydrogen molecules. A similar expression as in Eq. (5) was used but with a different polarizability coefficient α_{H^-} that we evaluate as 5.26 Å^3 based on quantum chemical calculations performed at the DFT level using the M06-2X functional and the aug-cc-pV5Z basis set. At the MP2/aug-cc-pV5Z level of theory, a slightly higher value of 5.92 Å^3 is found, but the energetic results were found to be barely affected by such a difference, largely owing to the high symmetry of most clusters that produces a vanishing field on the anion.

Having borrowed the intermolecular potential from earlier work, it remains to adjust the parameters of the isotropic potential between H_2 and H^-, leaving the orientation dependence to the charges carried out by individual atoms. This was achieved similarly as for the intramolecular H_2 potential by carrying out CCSD(T) calculations for the H_3^- system, placing H_2 at different distances from the H^- anion and varying its orientation as well, the energy being again evaluated in the CBS limit. The results of these calculations and the fitted potential are depicted in Fig. 2 for selected angles. In the least-square fitting process, more weight was given to the deepest parts of the potential corresponding to small angles θ, and the perpendicular configurations at θ approaching $\pi/2$ are not so well described. However, the general behavior is very satisfactory considering the very few number of parameters adjusted in the process and the lack of any explicit angular-dependent term: All variations with θ are caused by the partial charges included to describe the quadrupole moment.

As aforementioned, we also attempted to build a simplified united-atom model for anionic hydrogen clusters, replacing H_2 molecules by effective particles interacting with each other through the well-known Silvera-Goldman pair potential.[29] In such an approach, the interaction between H_2 and H^- is the sum of a repulsion-dispersion term and a polarization contribution in which the field originates from the anion alone. For this united-atom potential, we used the CCSD(T) data averaged over the molecular orientation θ, also superimposed in Fig. 2. In the united-atom potential, the hydrogen molecules lack a quadrupole and there is no polarization energy on the anion. The same expression for the repulsion-dispersion [Eq. (2)] and polarization [Eq. (4)] contributions on the hydrogen molecular centers as in the all-atom case were chosen, with parameters adjusted accordingly.

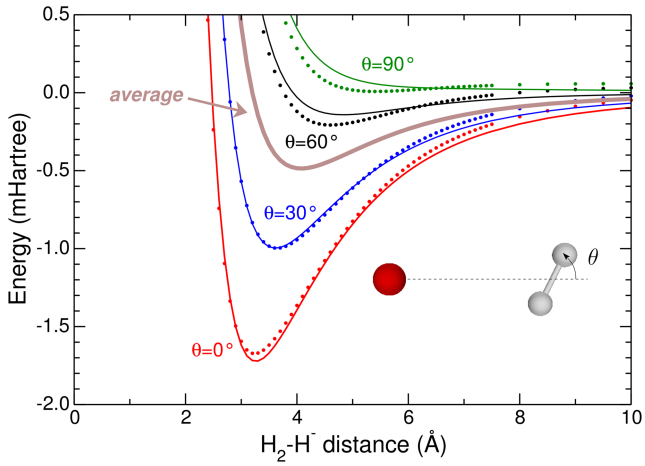


FIG. 2. Potential energy curves of the H_2–H^- system in its ground electronic state, as obtained from CCSD(T) calculations at the complete basis set limit (circles) or from the present polarizable potential (solid lines), for several angles between the H_2 molecular axis and the line joining H^- to the center of H_2. The potential averaged over all orientations is depicted as a solid brown line.

Already at this stage, it can be noticed that the H_2–H^- interaction is significantly stronger than the weak intermolecular potential between hydrogen molecules by 537 K versus 36 K. This effect is well known in the case of cationic impurities in helium droplets, as it causes the so-called snowball phenomenon in which neighboring solvent atoms freeze around the ion and become localized. In the present clusters, a similar behavior is expected with the hydrogen anion.

The parameters of the all-atom and united-atom potentials, original to the present work, are provided in Table I.

B. Path-integral molecular dynamics simulations

The structural properties of anionic hydrogen clusters $(H_2)_nH^-$ and $(D_2)_nD^-$ at low temperatures were explored using a variety of computational tools employing the potential energy surfaces described in Sec. II A. Our calculations have mostly relied on path-integral molecular dynamics simulations at thermal equilibrium, using a discretization (Trotter number) of $P = 128$ monomers at $T = 1$ K. The PIMD trajectories were thermalized using standard massive Nosé-Hoover thermostats and propagated with a time step of 0.2 fs. The total integration time over which observables were calculated and averages accumulated was 1 ns following an equilibration period of 200 ps. More details about the PIMD methodology can be found in earlier papers.[34–37]

TABLE I. Parameters of the all-atom and united-atom potentials, all expressed in atomic units.

Intramolecular potential			
V_0	a_{H_2}	r_{H_2}	δ_{H_2}
0.177 095	2.159 129	0.747 96	0.015 725 3
Intermolecular potential			
All-atom model			
A	b	C_6	C_8
1.030 577	0.867 754 5	184.326 35	0.119 049 66
United-atom model			
A	b	C_6	C_8
1.170 234 4	0.844 637	317.724 45	0.039 658
Damping parameters			
r_{cut} (*all-atom*)	r_{damp} (*all-atom*)	r_{cut} (*united-atom*)	r_{damp} (*united-atom*)
3.2	9.0	0	9.0
Atomic polarizability			
α_{H^-}			
35.5			

C. Observables

From the PIMD trajectories, the quantum energy at $T = 1$ K was evaluated using the virial estimator. Structural indicators were also considered to characterize the positions of the hydrogen molecules around the anionic center, namely, the radial distribution $\rho(r)$ of all hydrogen atoms but also the 2D angular distribution $p(\theta, \phi)$ of the molecular centers in the Euler angle space.

Although translational invariance is preserved by integration of the PIMD trajectories, rotational invariance is not and the system can experience some angular drift. In order to determine the spherical angles θ and ϕ, a reference frame was followed in time with the x axis pointing toward a specific molecular center $\bar{\mathbf{r}}_1$, where $\bar{\mathbf{r}}$ denotes the centroid position of the molecular center (average of positions of the two atoms comprising a molecule arbitrarily denoted as 1). A second molecule numbered as 2 was chosen in such a way that its center lies in the $z = 0$ plane. Care was taken in practice that molecules 1 and 2 are both nearest neighbors with the central hydrogen anion but not aligned with it. Along the course of the trajectory, the current configuration for each ring monomer was rotated with the purpose of placing the centers of molecules 1 and 2 aligned with the references axes, and the absolute angles θ and ϕ were evaluated at the molecular centers.

In addition to the energetic and structural observables, a systematic analysis of the inherent structures (ISs) in the vibrational wave function was conducted as a way to quantify the extent of vibrational delocalization. This energy landscape picture provides a connection between the degree of rigidity or fluxionality in the system and the magnitude of nuclear quantum effects. It has been used in the past to assist the interpretation of magic numbers in cationic neon clusters,[38] and more recently for polyaromatic hydrocarbons coated by helium clusters.[39]

D. Starting configurations

The PIMD trajectories were initiated from realistic structures obtained using global optimization conducted with the basin-hopping (BH) algorithm,[40] which consists of a Monte Carlo search in the configuration space of minima. In practice, molecular moves involving random translations and rotations were implemented, followed by the systematic local minimization of the potential energy. 10 000 minimizations were performed for each size n, and a zero temperature criterion was employed in which only moves that lower the energy are accepted. All classical structures reported in this work are true minima with no imaginary frequency indicative of a higher-order stationary point.

III. RESULTS AND DISCUSSION

The putative global minima obtained for small clusters containing between 1 and 12 hydrogen molecules are depicted in Fig. 3. At these small sizes, the present potential predicts stable structures that are essentially identical to those recently predicted by DFT[21] but were found to differ from early quantum chemistry calculations often carried at the Hartree-Fock level of theory.[18–20] In particular, the bent configuration of H_5^- is lower than the linear structure by about 3 meV, a result that is confirmed by single point calculations at the CCSD(T) level and in the CBS limit.

As their size increases, the classical structure of anionic hydrogen clusters exhibits a regular growth pattern in which the anion stays at the side, a shell of H_2 molecules building up around it and reaching completion at the icosahedral magic number of $n = 12$. Consistent with quantum chemical calculations that predict only minor charge transfer between the anion and the surrounding molecules,[21] strong electrostatic interactions are thus sufficient to explain the preferential orientation of the molecules toward the ion.

Treating the hydrogen molecules as flexible, the H_2 bond length is found to be generally affected by the proximity of the anion with a maximum elongation of about 1.5% with respect to the isolated molecule, already in the classically optimized structure but with an additional but minor contribution when quantum effects are incorporated.

For comparison, we also show in Fig. 3 the most stable structure found for the same cluster but using the united-atom potential in which hydrogen molecules are treated as point-like particles. Interestingly, and despite the overall arrangement remains icosahedral, it is now highly deformed with the anion lying outside.

The poor ability of the united-atom description indicates that the rotational average employed to derive the effective interaction is not accurate and fails in capturing the preferential orientation of the hydrogen molecules toward the anion. Interactions with the anion are thus essential not only in magnitude but also in directionality. Considering again the potential energy curves of Fig. 2, the different behaviors of the all-atom and united-atom models can be understood better since the potential averaged over all angles is reduced from 537 K to 158 K only. Such a weaker potential is no longer able to drive the impurity to the center of the cluster, hence the

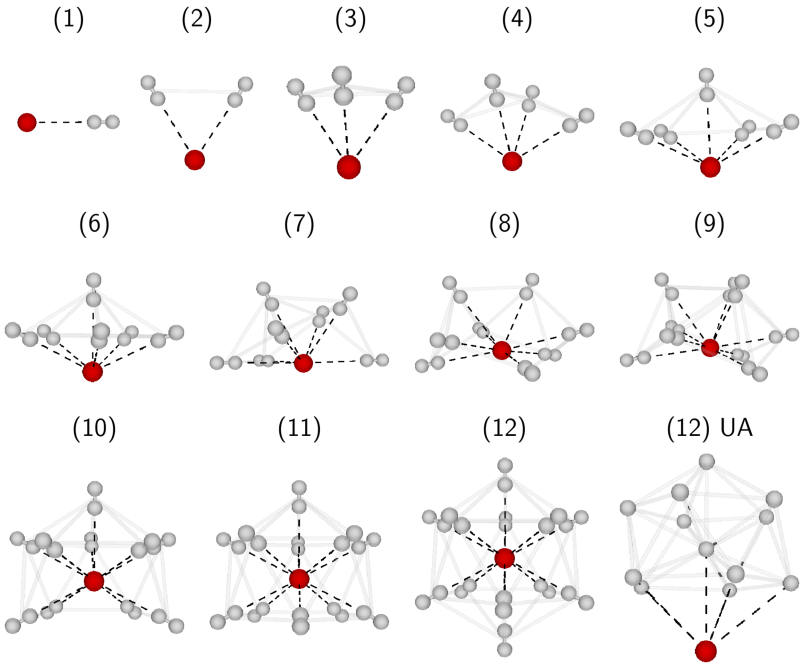


FIG. 3. Lowest-energy structures obtained for $(H_2)_nH^-$ clusters, $n = 1$–12, using the all-atom description and, for $n = 12$, the united-atom model. The anion is shown as a red ball, with the hydrogen atoms or entire molecules depicted as gray balls.

qualitatively different—and oversimplistic—results predicted by the united-atom model.

The variations of the (virial) quantum energy at 1 K for $(H_2)_nH^-$ and $(D_2)_nD^-$ with increasing size $1 \le n \le 54$ and per hydrogen molecule are represented in Fig. 4. Three regimes can be distinguished on these graphs, with essentially no qualitative difference upon deuteration but only a global shift of about 3 meV/molecule. At small sizes, the energy is dominated by the relatively strong H_2–H^- interactions and reaches a minimum at $n = 10$, above which the contribution of the more numerous but weaker H_2–H_2 interactions takes over. In large clusters, the later interactions eventually prevail and the binding energy should converge to the sublimation energies of 8.1 meV and 12.4 meV for bulk (fcc) hydrogen and deuterium, respectively.[29]

Dividing by n reveals the more remarkable sizes corresponding to complete shells arranged around the hydrogen

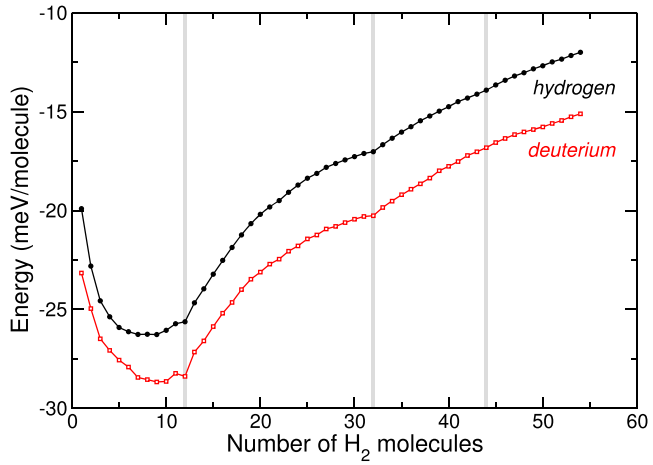


FIG. 4. Energy of $(H_2)_nH^-$ and $(D_2)_nD^-$ clusters as a function of n, as obtained from path-integral molecular dynamics simulations at $T = 1$ K. The gray vertical lines highlight the experimentally measured magic numbers.[5]

anion. These "magic" sizes occur at $n = 12$ and $n = 32$ with clear dips in the energy per molecule, and they match experimental abundances in mass spectra.[5] Cluster size effects[28] are also manifested in Fig. 4 with occasional nonmonotonic variations away from complete shells. Size 44, which was experimentally seen as also magic, does not stand out very much on the energy variations especially in the deuterium case. However, the remarkable feature of this cluster appears on its structure.

In Fig. 5, we compare the classical and quantum structures of selected $(H_2)_nH^-$ clusters, showing the global minima and the atomic density obtained from the PIMD trajectories after replacing all atoms in the reference frame having two molecules neighboring to the anion along the x axis and in the $z = 0$ plane, respectively. In addition to the energetically magic sizes 12 and 32, the nonmagic size 18 was chosen as well to illustrate the role of vibrational delocalization in defective structures. At $n = 12$ and $n = 32$, the most stable structures predicted by our potential belong to the I_h point group and consist of a single icosahedral shell and an additional dodecahedral shell above it. The next icosahedral shell brings 12 molecules aligned with the first 12 ones of the inner shell, but according to our calculation, this highly symmetric structure is not locally stable and relaxes by pushing away the outermost molecules from the icosahedral axes. The putative global minimum obtained for $n = 44$, depicted in Fig. 5(d), remains built on the two-shell, 32-molecule cluster of Fig. 5(c), but the extra molecules are misaligned and exhibit some degree of orientational disorder as well.

Once nuclear quantum effects are included at $T = 1$ K, the nuclear wave functions obtained for the clusters at $n = 12$ and 32 retain the icosahedral symmetry, each molecule keeping a well defined location. More surprisingly, the cluster at $n = 44$ now adopts the icosahedral symmetry with the 12 outermost molecules aligned with the 12 innermost molecules of the first shell.

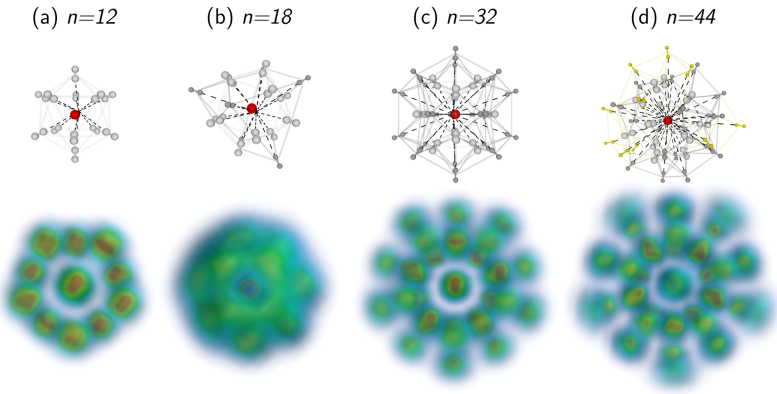


FIG. 5. Classical (top) and quantum (bottom) structures of selected $(H_2)_nH^-$ clusters.[43]

In contrast, the nonmagic cluster at $n = 18$ is rather symmetric (D_{3h} point group in its global minimum) but displays quite a delocalized wave function [see the bottom of Fig. 5(b)], which suggests that many molecules do not sit on their starting equilibrium position but instead fluctuate and migrate.

The degree of fluxionality and vibrational delocalization was quantified from the inherent structures locally minimized from the centroid positions. More precisely, we show in Fig. 6 the standard deviation around the average inherent structure energy for the two cluster types, as a function of their increasing size. This quantity exhibits strong nonmonotonic fluctuations with clear minima at the experimentally reported magic sizes $n = 12$, 32, and 44. The two smallest of these sizes are actually associated with zero fluctuations, indicating that the clusters behave solid-like at 1 K (see the inset of Fig. 6). This observation does not hold at $n = 44$, where residual fluxionality can be noticed with the wave function spanning over different classical minima. At $n = 18$, the large amount of delocalization found in Fig. 5(b) is reflected in a broadening of about 20 K in the inherent structure distribution. As shown in the inset of Fig. 6, the average IS energy also lies about 40 K above the classical global minimum, which suggests that the effective quantum structure of this cluster departs significantly from the highly symmetric geometry reported in Fig. 5(b). This phenomenon is similar to earlier reports of structural transitions induced by zero-point energy.[41,42] In larger clusters $n > 44$, inherent structures increasingly proliferate, suggesting as in the measurements[5] a more disordered liquid-like state.

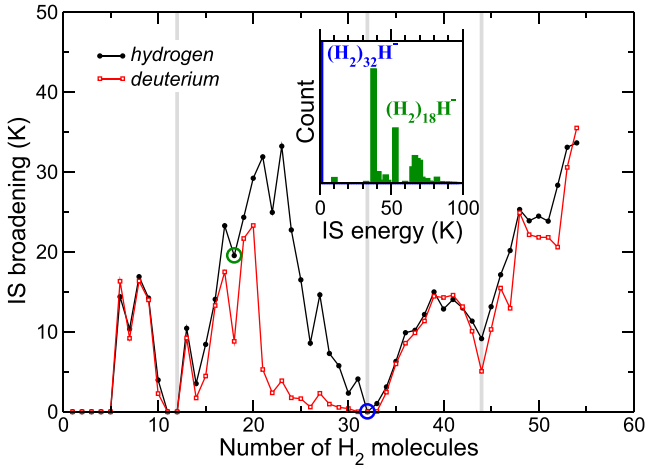


FIG. 6. Width of the inherent structure distributions obtained at the centroid configurations at 1 K, as a function of the number of H_2 or D_2 molecules in the cluster. The inset depicts two such distributions for $(H_2)_{18}H^-$ and $(H_2)_{32}H^-$.

While a correlation is found here between geometric stability and degree of delocalization in the energy landscape, care should be taken not to interpret low fluxionality as a signature of high energetic stability. This is especially clear in the case of deuterium clusters, which, as expected, generally display much lower vibrational delocalization and even nearly rigid-like clusters in the range $25 < n < 33$ (besides the magic number at $n = 32$) although not being associated with particularly stable geometric arrangements.

To further demonstrate that the vibrational wave functions sketched in Fig. 5 originate from highly symmetric structures, we have represented in Fig. 7 the (atomic) radial and (molecular) angular distribution functions of hydrogen molecules around the central anion, for the very same cluster sizes. The corresponding distributions for the classical structures, superimposed as histograms, display significantly shorter distances to the anion, as expected in the absence of nuclear delocalization. The two inner shells are particularly well resolved for the magic clusters, and noteworthily the absence of rotational motion of the innermost shell can be seen on the two peaks in the radial distribution near 3 and 3.7 Å. The peaks in the outermost shell are not so well resolved, and at $n = 18$ and 44, the exterior molecules even contribute as a shoulder. This indicates a much larger orientational freedom away from the anion, and in the large distance limit, isotropy should be recovered.

The angular distributions in the Euler angle space shed light on the degree of symmetry of the clusters. For the small icosahedral cluster at $n = 12$, twelve spots mark the 2D histogram around the classical equilibrium positions, confirming the rigid-like and weakly delocalized nature of this system. Conversely, at size $n = 18$, only one spot remains associated with a classical position at the center ($\theta = \phi = 0$), marking the molecule tagged as number 1 to be along the x axis of the reference frame when calculating the angular distributions. The very broad angular distributions obtained for this cluster is a manifestation of the large amplitude motion of the other molecules, hence a signature of qualitatively stronger delocalization in a more liquid-like picture.

In the two larger clusters, 32 spots can be clearly enumerated at the same positions, even for $n = 44$ where they notably deviate from the classical and not so symmetric positions. This

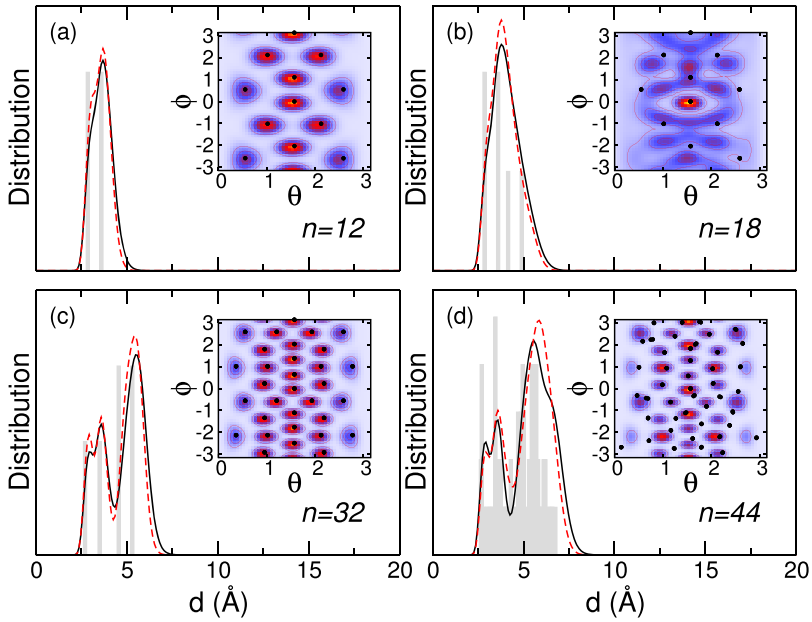


FIG. 7. Distribution of distances between hydrogen atoms and the hydrogen anion in selected $(H_2)_nH^-$ clusters: (a) $n = 12$, (b) $n = 18$, (c) $n = 32$, and (d) $n = 44$. The corresponding data for the deuterated clusters are superimposed with dashed red lines, and the gray vertical bars indicate the histograms for the classical structures. For each system, the inset highlights the angular distribution functions of H_2 molecules around the anion, Euler angles (θ, ϕ) being taken at the molecular centers. On these 2D plots, the angles in the classical structure are also depicted by black dots.

coincidence between the angular distributions in the 32- and 44-molecule clusters confirm that they share the same effective icosahedral symmetry and that indeed the three magic clusters follow the same growth pattern. The ability of the 44-molecule cluster to recover the icosahedral shape results from nuclear quantum effects, in which the outermost molecules are given more room through delocalization to move comfortably toward symmetric locations. The anisotropic arrangement that minimizes the classical energy is driven by nearest neighbor contacts and ignores the significant relaxation that especially affects the more distant molecules, which notably causes some expansion in intermolecular distances. The finite extension (or de Broglie wavelength) of the quantum particles thus helps the outer molecules to accommodate with the icosahedral symmetry of the inner shell, in agreement with the structure assumed to explain the experimental abundances.[5]

IV. CONCLUSIONS

Despite consisting only of protons and electrons, the physics and chemistry of charged hydrogen clusters are diverse and of possible relevance in hydrogen-rich environments such as those involved in energy storage or astrophysics. In the present work, we have addressed some fundamental properties of anionic hydrogen clusters, namely, their structure and energetics, in relation with recent mass spectrometry measurements of their relative abundances.[5] A dedicated flexible and polarizable potential was constructed based on the Darkrim-Levesque intermolecular potential, adding a Rydberg intramolecular potential for hydrogen molecules and placing polarizable sites on all molecular centers and the hydrogen anion. This potential features a very limited number of parameters and obviously was not designed for accurate energetic or spectroscopic properties; hence a lot of room is available for improvement along these lines. After adjustment of the parameters on high level quantum chemical calculations, the potential is found to predict multishell icosahedral structures with prominent stabilities found at 12 and 32 molecules. At such sizes, the molecules all point toward the charged impurity lying at the cluster center. The isotropically average united atom model is unable to account for such orientational effects and predicts qualitatively wrong structures instead.

Nuclear quantum effects, as included here through path-integral molecular dynamics simulations, appear important especially away from these magic numbers. Vibrational delocalization gives rise to some degree of fluxionality in the energy landscape, which could be quantified from the distribution of inherent structures. However, an interesting case was found at the size of 44 molecules, where the clusters adopt again a fully icosahedral multishell structure, consistent with the interpretation of experimental measurements[5] and despite the classical global minimum exhibiting a much lower symmetry. The icosahedral arrangement at this specific size was found to be largely due to quantum effects that lower the atomic density and stabilize the outermost shell.

The present study was thus able to further support the simple geometric interpretation of experimentally measured relative abundances in $(H_2)_nH^-$ clusters[5] and shed light onto the importance of nuclear quantum effects for these systems. In agreement with the experiment, we have not found qualitative differences between hydrogenated and fully deuterated compounds. However, in our modeling, we have ignored the possible contribution of nuclear spin statistics, and such quantum effects could become important especially away from the impurity where interactions are weaker and delocalization is enhanced.

Another issue worth pursuing is mixed clusters composed of hydrogen and deuterium molecules, interacting with an anionic impurity H^- or D^-. Theoretical studies of neutral clusters of *para*-hydrogen and *ortho*-deuterium have shown interesting phase separation behavior,[9,44–46] and the presence of a dopant could well modify this behavior. Mixed hydrogen/deuterium clusters are also important in astrochemistry because the D/H ratio in the galaxy is about 10^4 lower than its abundance on Earth.[47] Although not directly amenable to mass spectrometry characterization, such an extension would also

be useful to get deeper insight into the mechanisms responsible for separation between the two isotopes, with possible long-term applications into quantum sieving.[48,49]

SUPPLEMENTARY MATERIAL

See supplementary material for Fortran routines to calculate the energy and gradient of the potential for $(H_2)_nH^-$ clusters, as well as the most stable structures found for these clusters at $n = 12$, 18, 32, and 44.

ACKNOWLEDGMENTS

Financial support through a joint grant from CNRS/TUBITAK is gratefully acknowledged.

[1] D. Stevenson and J. Hirschfelder, J. Chem. Phys. **5**, 933 (1937).
[2] J. Stärk and W. Meyer, Chem. Phys. **176**, 83 (1993).
[3] M. Ayoux, O. Dulieu, R. Guérout, J. Robert, and V. Kokooline, J. Chem. Phys. **132**, 194309 (2010).
[4] W. Wang, A. K. Belyaev, Y. Xu, A. Zhu, C. Xiao, and X.-F. Yang, Chem. Phys. Lett. **377**, 512 (2003).
[5] M. Renzler, M. Kuhn, A. Mauracher, A. Lindinger, P. Scheier, and A. M. Ellis, Phys. Rev. Lett. **117**, 273001 (2016).
[6] R. Prosmiti, A. A. Buchachenko, P. Villareal, and G. Deltago-Barrio, Theor. Chem. Acc. **106**, 426 (2001).
[7] G. Moyano and M. Collins, J. Chem. Phys. **119**, 5510 (2003).
[8] H. J. Maris, G. M. Seidel, and T. E. Huber, J. Low Temp. Phys. **51**, 471 (1983).
[9] F. Mezzacapo and M. Boninsegni, J. Phys. Chem. A **115**, 6831 (2011).
[10] A. Cruz and G. E. López, Phys. Lett. A **378**, 1375 (2014).
[11] P. Drossart, J.-P. Maillard, J. Caldwell, S. J. Kim, J. K. G. Watson, W. A. Majewski, J. Tennyson, S. Miller, S. K. Atreya, J. T. Clarke, J. H. Waite, Jr., and R. Wagener, Nature **340**, 539 (1989).
[12] T. R. Geballe, M.-F. Jagod, and T. Oka, Astrophys. J. **408**, L109 (1993).
[13] T. R. Geballe and T. Oka, Nature **384**, 334 (1996).
[14] B. J. McCall, T. R. Geballe, K. H. Hinkle, and T. Oka, Science **279**, 1910 (1998).
[15] P. H. Aciolo, Z. Xie, B. J. Braams, and J. M. Bowman, J. Chem. Phys. **128**, 104318 (2008).
[16] A. Aguado, P. Barragan, R. Prosmiti, G. Delgado-Barrio, P. Villareal, and O. Roncero, J. Chem. Phys. **133**, 024308 (2010).
[17] O. Heber, R. Golser, H. Gnaser, D. Berkovits, Y. Toker, M. Eritt, M. L. Rappaport, and D. Zajfman, Phys. Rev. A **73**, 060501 (2006).
[18] A. M. Sapse, M. T. Rayez-Meaume, J. C. Rayez, and L. J. Massa, Nature **278**, 332 (1979).
[19] J. C. Rayez, M. T. Rayez-Meaume, and L. J. Massa, J. Chem. Phys. **75**, 5393–5397 (1981).
[20] K. Hirao and S. Yamabe, Chem. Phys. **80**, 237 (1983).
[21] L. Huang, C. F. Matta, and L. Massa, J. Phys. Chem. **115**, 12445 (2011).
[22] L. A. der Lan, P. Bartl, C. Leidlmair, R. Jochum, S. Denifl, O. Echt, and P. Scheier, Chem.- Eur. J. **18**, 4411 (2012).
[23] T. MacFarland, S. A. Vitiello, L. Retatto, G. V. Chester, and M. H. Kalos, Phys. Rev. B **50**, 13577 (1994).
[24] E. Coccia, E. Bodo, F. Marinetti, F. A. Gianturco, E. Yildrim, M. Yurtsever, and E. Yurtsever, J. Chem. Phys. **126**, 124319 (2007).
[25] E. Coccia, E. Bodo, and F. A. Gianturco, Europhys. Lett. **82**, 23001 (2008).
[26] N. Issaoui, K. Abdessalem, H. Ghalla, S. J. Yaghmour, F. Calvo, and B. Ouija, J. Chem. Phys. **141**, 174316 (2014).
[27] E. Coccia, F. MArinetto, E. Bodo, and F. A. Gianturco, ChemPhysChem **9**, 1209 (2008).
[28] J. Jortner, Z. Phys. D: At., Mol. Clusters **24**, 247 (1992).
[29] I. F. Silvera and V. V. Goldman, J. Chem. Phys. **69**, 4209 (1978).
[30] R. J. Hinde, J. Chem. Phys. **128**, 154308 (2008).
[31] F. Darkrim and D. Levesque, J. Chem. Phys. **109**, 4981 (1998).
[32] D. Levesque, A. Gicquel, F. Lamari Darkrim, and S. Beyaz Kayiran, J. Phys.: Condens. Matter **14**, 9285 (2002).
[33] T. N. Olney, N. M. Cann, G. Cooper, and C. E. Brion, Chem. Phys. **223**, 59 (1997).
[34] A. Pérez, M. E. Tuckerman, and M. H. A. Müser, J. Chem. Phys. **130**, 184105 (2009).
[35] A. Witt, S. D. Ivanov, M. Shiga, H. Forbert, and D. Marx, J. Chem. Phys. **130**, 194510 (2009).
[36] F. Calvo and E. Yurtsever, J. Chem. Phys. **144**, 224302 (2016).
[37] F. Calvo and E. Yurtsever, J. Chem. Phys. **145**, 084304 (2016).
[38] F. Calvo, F. Y. Naumkin, and D. J. Wales, Chem. Phys. Lett. **551**, 38 (2012).
[39] F. Calvo, J. Phys. Chem. A **119**, 5959 (2015).
[40] D. J. Wales and J. P. K. Doye, J. Phys. Chem. A **101**, 5111 (1997).
[41] F. Calvo, J. P. K. Doye, and D. J. Wales, J. Chem. Phys. **114**, 7312 (2001).
[42] C. J. Burnham, S. S. Xantheas, M. A. Miller, B. E. Applegate, and R. E. Miller, J. Chem. Phys. **117**, 1109 (2002).
[43] The 3D density plots have been constructed using the Mayavi2 suite of Python scripts, P. Ramachandran and G. Varoquaux, IEEE Comput. Sci. Eng. **13**, 40 (2011).
[44] D. Scharf, G. J. Martyna, and M. L. Klein, Chem. Phys. Lett. **197**, 231 (1992).
[45] J. E. Cuervo and P.-N. Roy, J. Chem. Phys. **131**, 114302 (2009).
[46] S. Shim and Y. Kwon, J. Low Temp. Phys. **158**, 281 (2010).
[47] T. J. Millar, Planet. Space Sci. **50**, 1189 (2002).
[48] J. J. M. Beenakker, V. D. Borman, and S. Y. Krylov, Chem. Phys. Lett. **232**, 379 (1995).
[49] H. Oh and M. Hirscher, Eur. J. Inorg. Chem. **27**, 4278 (2016).